A Versatile Leaky-Wave Antenna Based on Stub-Loaded Rectangular Waveguide: Part III—Comparisons with Measurements

Mikio Tsuji, *Member, IEEE*, Hiroshi Shigesawa, *Fellow, IEEE*, Fabrizio Frezza, *Senior Member, IEEE*, Paolo Lampariello, *Fellow, IEEE*, and Arthur A. Oliner, *Life Fellow, IEEE*

***Abstract*— Parts I and II of this three-part series of papers presented the theory for this new type of leaky-wave antenna. Part III now describes the measurements that verify the validity of the theoretical expressions. Measurements were made both at millimeter wavelengths and in the X-band frequency range and of two different quantities: the propagation wavenumbers β and α and radiation patterns. Comparisons were made with numerical values obtained from the theoretical expressions derived in Parts I and II and very good agreement was found in all cases.**

***Index Terms*—Leaky-wave antennas.**

I. Introduction

PARTS I [1] and II [2] of this three-part series of papers presented the theory for this new type of leaky-wave antenna; Part III now describes the *measurements* that verify the theoretical predictions.

Measurements were made in two different frequency ranges: in the millimeter-wave range from 40 to 60 GHz and in the X-band frequency range from roughly 8 to 12 GHz. Different antenna structures needed to be built for each frequency range, of course, and the specific *structures* are described in Section II. The millimeter-wave measurements were performed by the team in Japan and the measurements at X-band were conducted later and independently by the team in Italy. As a result, the specific measurement methods used by each team differ somewhat from each other; for example, the team in Japan employed a sliding short, whereas the team in Italy used a sliding probe. The *measurement methods* themselves are described in Section III.

Two types of quantities were measured: the propagation wavenumbers β (the phase constant) and α (the leakage constant) and radiation patterns. The measured results are compared with numerical values calculated from the theoretical expressions derived in Parts I and II and the comparisons for the wavenumbers and for the radiation patterns are presented in Sections IV and V, respectively. The wavenumber results for the measurements at millimeter wavelengths agreed excellently with the theoretical values on the average, but showed some scatter in the points. Since the scatter could be due to the difficulty in making precise measurements at these small wavelengths, we decided to perform corresponding measurements (and calculations) in the X-band frequency range where all dimensions are larger by about a factor of five.

The stub guide on the antenna measured at millimeter wavelengths possessed very wide flanges (essentially an infinite ground plane). The antenna for the X-band measurements had small flanges, plus a provision for adding side flanges to produce very wide flanges instead. We were therefore able to determine quantitatively the differences in the *propagation wavenumber* values due to the use of narrow flanges versus very wide flanges. We also calculated the differences theoretically when very wide flanges are used to terminate the stub guide and when a pair of baffles is employed instead. For those theoretical values we used the expressions derived in Part II. We found that the values of β are influenced negligibly by changes in the type of termination, but that the values of α do show changes, indicating that we must pay attention in the design to the geometry of the termination on the stub guide. These results are discussed in Section IV-B.

In Part I we discussed two theoretical approaches, the mode-matching method, and the new approach based on a novel equivalent network for the E-plane tee junction and we demonstrated that calculated values from the two methods agreed extremely well with each other. In the comparisons with measurements for β and α, the theoretical values for comparison with the millimeter-wave measurements employed the mode-matching method and those for the X-band range used the new network approach. As shown in Section IV, the agreements between the measured and the theoretical values are *very good* in *all* cases, thereby verifying that the theoretical expressions in Parts I and II provide accurate and reliable numerical results.

Radiation pattern measurements were taken in both the millimeter-wave and X-band frequency ranges, but in both cases, the distances between the transmitting and receiving antennas were too short to permit far-field measurements to be taken. As a result, the measurements had to be made in the

Manuscript received April 30, 1996; revised December 2, 1997. This work was supported by the Ministero dell'Università e della Ricerca Scientifica e Tecnologica and the Consiglio Nazionale delle Ricerche, Italy, by Doshisha University's Research Promotion Fund, Japan, and by the United States Air Force RADC under Contract F19 628-84-K-0025.

M. Tsuji and H. Shigesawa are with the Department of Electronics, Doshisha University, Kyoto, 61003 Japan.

F. Frezza and P. Lampariello are with the Department of Electronic Engineering, "La Sapienza" University of Rome, Rome, 00184 Italy.

A. A. Oliner is with the Department of Electrical Engineering, Polytechnic University, Brooklyn, NY, 11201 USA.

Publisher Item Identifier S 0018-926X(98)05783-4.

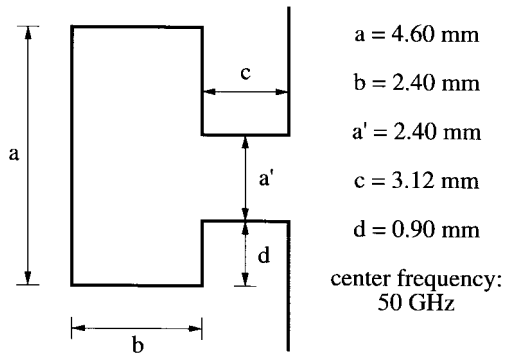

Fig. 1. Cross section of the stub-loaded rectangular guide antenna for which measurements were taken at millimeter wavelengths (40 to 60 GHz).

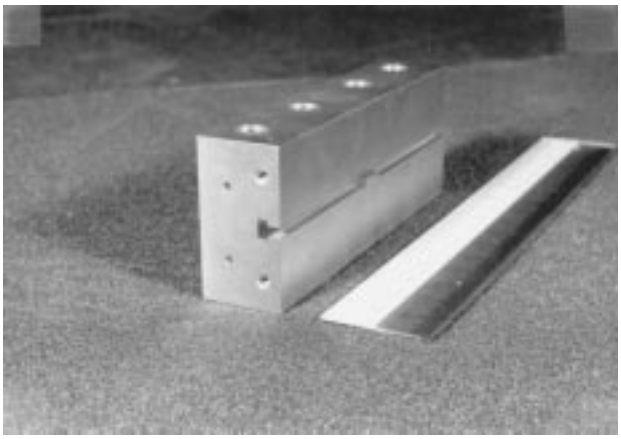

Fig. 2. Photograph with a three-dimensional view of the actual antenna that was measured at millimeter wavelengths, showing that the antenna aperture is 10 cm long. The projection appearing part way down the guide is a moveable short circuit.

near field. For the millimeter-wave range, calculations were also made of the near-field patterns and the comparisons with the measured patterns, as seen in Section V, showed *very good agreement*, providing a further verification of the validity of the theoretical expressions in Parts I and II.

II. The Structures Under Measurement

Two different structures were fabricated: one for measurements at millimeter wavelengths and the other for measurements at X-band. The details for each of the two structures are given below.

A. For Millimeter Wavelengths

A cross-section sketch of the stub-loaded rectangular waveguide antenna that was measured at frequencies from 40 to 60 GHz is presented in Fig. 1, together with the dimensional details. A photograph of the structure is shown in Fig. 2 in which it is seen that the guiding portion is channeled out of a solid block of brass. It is also seen that the stub guide of length c is terminated by very wide flanges (essentially an infinite ground plane).

From Fig. 1 we see that the stub-guide length c is equal to 3.12 mm, which turns out to be roughly a half free-space wavelength at the mid-frequency 50 GHz. That length is reasonably short so that we should be able to avoid the peculiar coupling problems to another leaky mode that we discussed in Part II, Section III-B. In Section IV below, we demonstrate that such problems are indeed avoided here.

The ruler in the photograph in Fig. 2 indicates that the length of the antenna aperture is 10.0 cm. Note that a projection appears part way down the guide. It is a moveable short-circuit plunger that has the same cross-section dimensions as the antenna itself; it was used to obtain the values of α and β by measuring the variation in reflected power produced by changing the distance between the input plane and the moveable short. The details of the measurement procedure are presented in the next section.

The antenna was fed from a rectangular waveguide of almost the same dimensions as the main guide section of the antenna. The feed waveguide is WR 19 with nominal cross-section dimensions 4.775 mm $\times$ 2.388 mm; the antenna's cross-section dimensions are 4.60 mm $\times$ 2.40 mm. The electrical mismatch at the junction between the two structures was found to be very small, but it was taken into account in the measurement procedure.

The feed waveguide's cutoff frequency is 31.4 GHz and its recommended operating range is 39.3 to 59.7 GHz. We took measurements from 40 to 60 GHz of both the propagation wavenumbers β and α and the radiation patterns. The wavenumber results are discussed in Section IV and the radiation patterns in Section V.

B. For the X-Band

The shape of the cross section of the X-band version is of course the same as the one shown in Fig. 1. The dimensions for the X-band structure are: $a = 23.00$ mm; $b = 11.95$ mm; $a' = 11.95$ mm; $c = 15.65$ mm; $d = 4.55$ mm.

A photograph of the structure with a centimeter scale is seen in Fig. 3, which shows that tapers are employed to allow a gradual transition between the feed-guide portions and the central antenna section. In the millimeter-wave version, a direct junction was employed, but the discontinuity effect was very small. The measurements of the propagation wavenumber were made using the sliding probe shown in Fig. 3, but its position was varied automatically by means of a small motor. The total length of the antenna portion is 50.3 cm.

Two types of flanges were used with this structure, one narrow and the other very wide, in order to determine the differences produced in the wavenumber values (β and α). The differences that were found are discussed in Section IV. The structure shown in Fig. 3 corresponds to the narrow-flange case. As seen, the two sides are not quite symmetrical (because the radiating aperture must be located off center); the flange on one side is 15.0 mm wide while that on the other side is 21.5 mm wide. To produce very wide flanges (the equivalent of a ground plane), an additional extension with a width of 20.0 cm, was placed on each side of the original structure.

The X-band feed guide is designed to cover the frequency range from 8.2 to 12.4 GHz and measurements of the wavenumbers and radiation patterns were taken from 8.5 to 12.0 GHz.

Fig. 3. Photograph of the antenna that was measured in the X-band frequency range. Note the sliding probe and the tapers at each end.

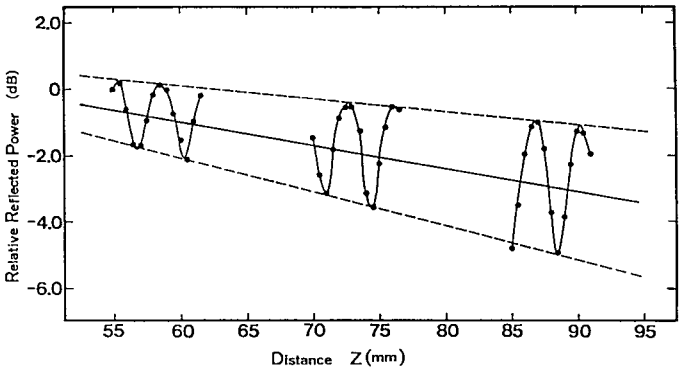

Fig. 4. Typical plot of the measured relative reflected power in decibels at 54.8 GHz as a function of the distance of the moveable short to the junction between the antenna and the feed guide. The dimensions of the antenna are those indicated in Fig. 1.

III. Methods of Measurement

As indicated in the Introduction, measurements were made of the propagation wavenumbers β and α and of radiation patterns on two different antenna structures—one for the millimeter wave range and the other for the X-band range. Since the measurement setups and the measurement procedures are different for wavenumbers and for radiation patterns, they are discussed separately below.

A. Propagation Wavenumbers

The procedures used for the measurement of the phase constant β and the attenuation constant α are slightly different for the millimeter wave range and for the X-band range since the moveable short shown in Fig. 2 was used in the millimeter wave measurements and the sliding probe seen in Fig. 3 was used for the X-band measurements. All of the measurements were made in an anechoic chamber and utilized a sweep-frequency source and a network analyzer.

The wavenumbers β and α were measured in the 40–60-GHz frequency range by employing the moveable short (shown in Fig. 2) and measuring the reflected power as a function of the distance of the moveable short from the junction between the feed waveguide and the antenna structure. Presented in Fig. 4 is a typical plot of the measured relative reflected power plotted on a logarithmic scale as a function of the distance of the moveable short from the junction mentioned above. The total antenna aperture length is 100 mm. The oscillation in the reflected power is due to the interference between the reflected wave from the moveable short and the wave reflected back from the small discontinuity present at the junction between the feed guide and the antenna. (Even though the reflection from the discontinuity at the feed junction is very small, it must be realized that the amount of power reflected from the moveable short circuit is also quite small by the time it returns to the feed junction. The power that first enters the antenna region is reduced by leakage (radiation) *twice*—once going out and again after reflection by the moveable short circuit.) We applied Deschamps' reflection-coefficient procedure [3] to determine accurately the scattering-matrix parameters that characterize that small discontinuity and then subtracted out its effect at each point to determine the true reflection coefficient at each distance z in Fig. 4. When that step is performed, one obtains the solid straight line shown roughly midway between the two dashed straight lines. However, a result that is almost the same is achieved by simply taking the average of the slopes indicated by the two dashed lines—a step that is valid if the reflection from the feed discontinuity is sufficiently small.

The value of the attenuation constant α in dB/mm is determined by taking one half of the slope of the solid line mentioned above. To find α/k_o, the above value for α is divided by 8.686 times the appropriate value of k_o. The distance between neighboring maxima or minima is equal to $\lambda_g/2$; a measurement of this distance thus yields π/β, with β in units of mm^{-1}.

The measurements at X-band employed the sliding probe shown in Fig. 3 in most cases, where the probe was moved automatically by means of a small motor. For the measurement of β, two methods were used; both utilized the sliding probe and the results agreed very well with each other. In the first method, a short circuit was placed at the output port of the antenna structure and the standing wave pattern was measured at a series of frequencies using the sliding probe. From these patterns, one readily obtains the guide wavelength from which the value of β is found as indicated above. In the second method, a matched termination is placed at the end of the antenna and the phase at the sliding probe is measured as the position of the sliding probe is varied. From the slope of the phase response, one readily finds the value of β.

For the measurement of α at X-band, two methods were again used and the results again agreed very well. In one method, a matched load was placed at the end of the antenna and the amplitude at the sliding probe was measured as the position of the sliding probe was varied. From one-half of the slope of these data on a semilog plot, one finds α in decibels per unit length and then the value of α/k_o is obtained as indicated above in connection with the measurements at millimeter wavelengths. In the second method, which does not employ the sliding probe, one measures the frequency response of the amplitude $|S_{21}|$ of the whole antenna structure considered as a two-port device. Further details regarding the measurement methods used for the X-band range appear in a paper in Italian and were presented at a national conference in Italy [4].

The contribution to the attenuation constant due to metal losses was found to be very small compared to the measured values of α so that we have taken the measured values to be equal to the leakage constant in all the cases.

B. Radiation Patterns

Radiation patterns were measured in both the millimeter wave and X-band frequency ranges. For the millimeter wave range, a receiving pick-up horn was used to sample the radiated field and the horn was located on a boom that swung through the required range of angles. The surrounding area was covered with absorbing material. The antenna structure was fed at one end and a matched load was placed at the other end.

For the X-band range, the leaky-wave antenna was employed as a receiving antenna (rather than a transmitting antenna) and it was placed on a low-dielectric constant support, which, in turn, was located on a rotating positioner hidden under the floor of the anechoic chamber and surrounded by absorbing material. The transmitting horn antenna was situated on a low-dielectric constant support and was located appropriately using a sliding positioner.

A key problem that arose in connection with all of these pattern measurements is that the distance between the antenna and the horn was too short to permit far-field measurements. The measurements had to be taken in the *near field*, where the patterns are not as simple or pretty, but near-field pattern calculations were made for the millimeter wave range that showed very good agreement with the measured data. These comparisons and further details are presented in Section V.

IV. Propagation Wavenumbers

A. Preliminary Theoretical Calculations

In an actual stub-loaded rectangular-waveguide leaky-wave antenna where the stub guide is of finite length c (see Fig. 1), it is possible to excite another leaky mode (the channel-guide leaky mode) in addition to or instead of the desired leaky mode and it is possible to couple these two modes together. The explanation for these effects is presented in [2, pt. II, Section III-B] and in greater generality in a separate paper [5]. The proper design of the antenna thus requires some preliminary theoretical calculations to assure us that first, the leaky mode we are measuring is indeed the desired leaky mode, and second, the two leaky modes are not coupled together.

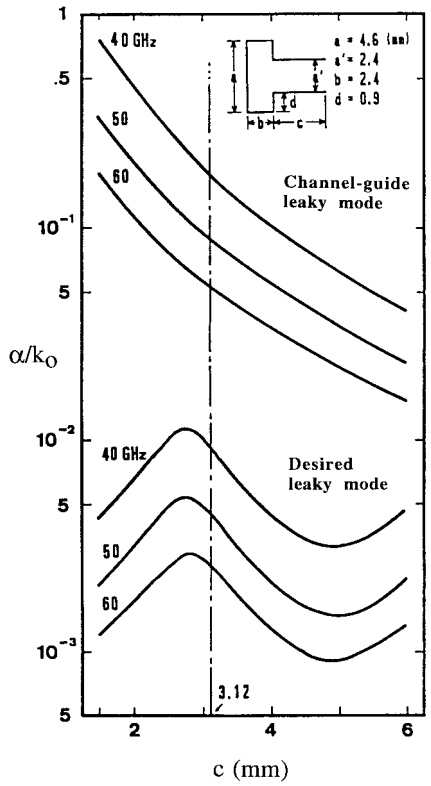

Fig. 5. Preliminary theoretical calculations of the normalized leakage constant as a function of stub-guide length for both the desired and channel-guide leaky modes for three different frequencies in the millimeter-wave range.

Such preliminary calculations for the propagation wavenumbers are discussed below, but only for the 40–60-GHz frequency range. After that, in order to clarify the different physical behaviors of the two different leaky-mode types, vector electric field plots are presented for both mode types.

1) Wavenumber Considerations: Preliminary theoretical calculations of the type referred to above for the dimensions of the specific antenna to be measured, are presented in Fig. 5 for α/k_o as a function of the stub length c at three different frequencies (40 GHz: low end; 50 GHz: mid-range frequency; and 60 GHz: high end). It is seen that the two leaky modes, the desired leaky mode and the channel-guide leaky mode, do *not* couple for this set of parameters since the values of α/k_o for the two mode types are well separated from each other.

2) Vector Field Distributions: Using the mode-matching calculation procedure, we were able to obtain information regarding the electric field strengths and their directions at any interior point in the guiding structure. Therefore, we prepared a grid with many points and determined the vector electric field strengths at each of those grid points. The resulting computer-plotted patterns within the leaky-waveguide cross section are presented in Figs. 6 and 7 for the desired leaky mode and the channel-guide leaky mode, respectively, at a frequency of 40 GHz.

It is interesting to see the influence of asymmetry in both of the cases. In Fig. 6 for the desired mode, the field distribution

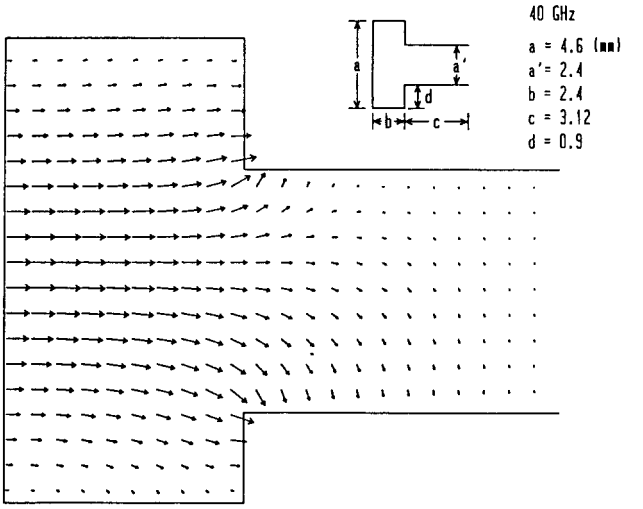

Fig. 6. Vector electric field plot for the desired leaky mode, showing the field strengths and the field directions at each point in a grid of many points.

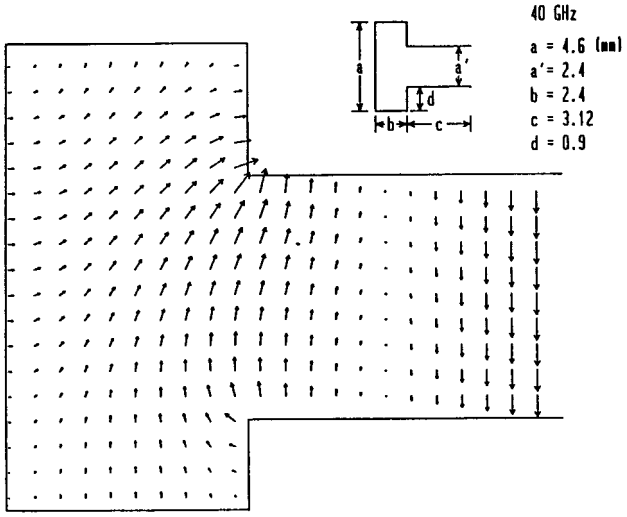

Fig. 7. Same as for Fig. 6, but for the channel-guide leaky mode.

in the main guide is clearly similar to what we would expect for the lowest mode in rectangular waveguide; the asymmetric stub guide is seen to produce a small amount of oppositely polarized (horizontal) field, which then maintains itself as one moves transversely along the stub guide while the original (vertical) polarization content steadily decreases. The leakage rate is small here, however, so that the details of the field at the radiating open end are not very clear. In Fig. 7, the field distribution for the channel-guide leaky mode is seen to be *very different*, with predominantly the opposite polarization and with a phase reversal in the stub guide. The electric field in the aperture is also quite strong, consistent with the fact that its leakage constant is more than an order of magnitude higher than that for the desired mode. Also, the fields in the vicinity of the junction between the main and stub guides resemble what one would expect for the dominant mode in parallel-plate guide incident on a transverse change in height. The field lines are disturbed only a little in the stub guide, and the bulk of the field line curvature occurs in the main guide portion.

B. Measured Results and Comparisons with Theory

The structures that were measured at millimeter wavelengths and over the X-band frequency range are described in detail in Section II; the methods used to measure the propagation wavenumbers in each of these ranges are discussed in Section III-A.

Two alternative theoretical approaches were employed in the numerical calculations: the well-known mode-matching procedure and the new approach based on a novel equivalent network for the E-plane tee junction. In the comparisons with measurements discussed below, the theoretical values for the 40–60-GHz frequency range were obtained using the mode-matching method, whereas the computations for the X-band frequency range employed the equivalent network based on the tee junction. However, it was shown in Section III-C of Part I that the numerical values for the wavenumbers obtained from these two methods agreed excellently with each other and that both can be viewed as accurate and reliable.

The preliminary theoretical calculations in Section A (above) hold when a pair of baffles terminates the stub guide on the antenna structure, as may be seen in the inset on Fig. 5 and on the structures in Figs. 6 and 7. Since those theoretical values were obtained to serve as a guide to design, the precise values were not as important as the behavior trends. Now, however, we wish to make careful comparisons between theoretical values and measured results so that it becomes necessary to take into account the actual structural details. In fact, in connection with the X-band measurements and calculations, the differences were determined between narrow and wide flanges and between wide flanges and a pair of baffles. The changes in the theory that must be taken into account when flanges are used instead of a pair of baffles have been treated in detail in Part II. Although the application there was made directly to the tee-junction network approach, the identical expressions for the terminal admittances can be (and were) incorporated into the mode-matching procedure.

1) The 40–60-GHz Frequency Range: The structure for which measurements in this range were taken possessed wide flanges (a ground plane) at the end of the stub guide, as indicated in Fig. 1 and as seen in Fig. 2. The measurements were made using the sliding short shown in Fig. 2 and the technique described in Section III-A.

The comparisons between the measured and the theoretical values for the normalized wavenumbers β/k_o and α/k_o for this structure in the 40–60-GHz frequency range are shown in Fig. 8. The measured data are presented in that figure as the black dots and the solid and dashed curves represent the theoretical calculations made using the mode-matching procedure, incorporating the expression for the flange termination presented in Part II. The solid lines correspond to the desired leaky mode and the dashed lines to the channel-guide leaky mode. The first point to be noted is that the mode that was excited in the antenna is, without question, the desired leaky mode. Since the antenna was fed by the input rectangular guide in straightforward fashion, the measured results indicate that the potential presence of the channel-guide leaky mode

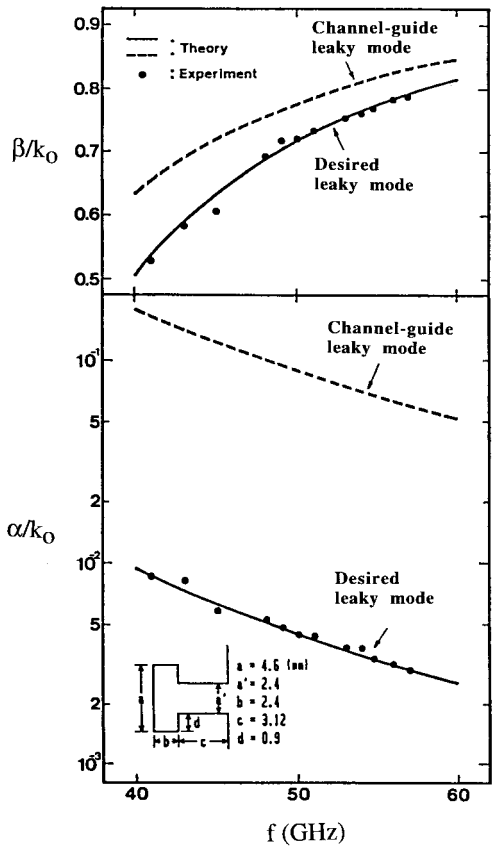

Fig. 8. Comparisons of theoretical and measured values for the normalized phase and leakage constants of the stub-loaded rectangular-guide antenna as a function of frequency from about 40 to 60 GHz.

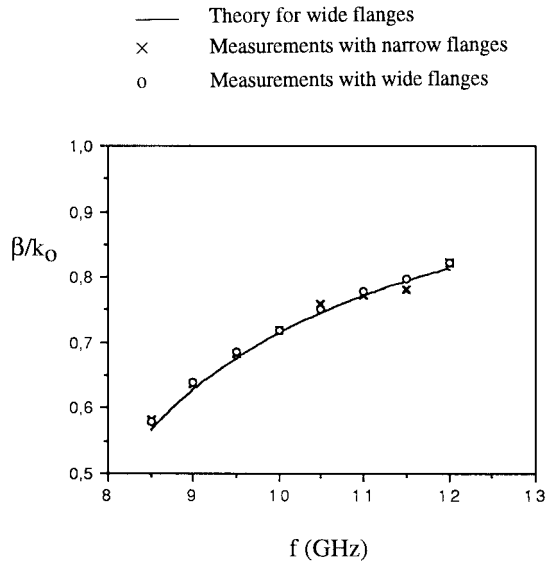

Fig. 9. Comparisons between measured and theoretical values for the normalized phase constant as a function of frequency for the X-band range. Separate measurements were taken for narrow flanges and for wide flanges.

can be ignored unless the two leaky-mode types are actually coupled together, which can happen only for large leakage rates and an excessively long stub guide, as discussed in Part II, Section III-B.

We next observe that *very good agreement* has been obtained between the measured and theoretical values for both β/k_o and α/k_o. The measured data show some scatter, however, which we attribute to the small wavelength and the attendant difficulty in making precise measurements in this frequency range. For this reason, we decided to perform corresponding measurements (and calculations) in the X-band frequency range where all dimensions are larger by about a factor of five.

2) The X-Band Frequency Range: A photograph of the structure under measurement in the 8.5 to 12.0 GHz frequency range is shown in Fig. 3. Two types of flanges were used to terminate the stub guide—the narrow flanges shown in Fig. 3 and much wider flanges, which were produced by using additional extensions. Further details are given in Section II-B. The measurement methods, which were based primarily on the use of the sliding probe seen in Fig. 3, are described in Section III-A.

The theoretical calculations made for comparison with the measured results employed the equivalent network based on the tee junction, taking into account the presence of the flanges and, in one calculation, a pair of baffles instead of flanges. The expressions used were exactly those presented in Part II.

Let us first consider Fig. 9, which presents a comparison between measured and theoretical results for the normalized *phase constant* β/k_o, where the solid curve represents the theoretical calculations using the theory for wide flanges. There are two sets of measured data; $\times$ signifies the results when the *narrow* flanges shown in Fig. 3 are used and the small circles represent the values found when an additional extension of width 20.0 cm was placed on each side of the original structure to create *very wide* flanges.

An inspection of Fig. 9 indicates that some scatter is still present in the measured values, but it is less than what was obtained at millimeter wavelengths. When the points marked $\times$ are compared with those indicated by small circles, we note that there is no systematic difference between them; if there is any it is obscured by the scatter. We therefore obtain an important conclusion: with respect to β/k_o, the measured values for narrow flanges are negligibly different from those for very wide flanges.

From Fig. 9, we also observe that the measured results *agree very well* with the theoretical results given by the solid curve. In Fig. 8, the agreement involved theoretical values calculated using the mode-matching method; in Fig. 9, the theoretical values were obtained via the tee-junction equivalent network, so that this agreement independently verifies the validity of that approach. Since the measured results for narrow flanges and for very wide flanges are essentially identical with respect to the β/k_o values, we wondered how the theoretical results would differ when the wide flanges were replaced by a pair of baffles. We found that the difference was essentially negligible; the largest difference numerically was about 0.2%—an amount that would not be visible on a graphical plot.

The corresponding information for the normalized *leakage constant* α/k_o appears in Fig. 10. The most important observation is that the differences that were negligible for β/k_o are now noticeable for α/k_o. With respect to the measured values, we see that despite a small amount of scatter, there

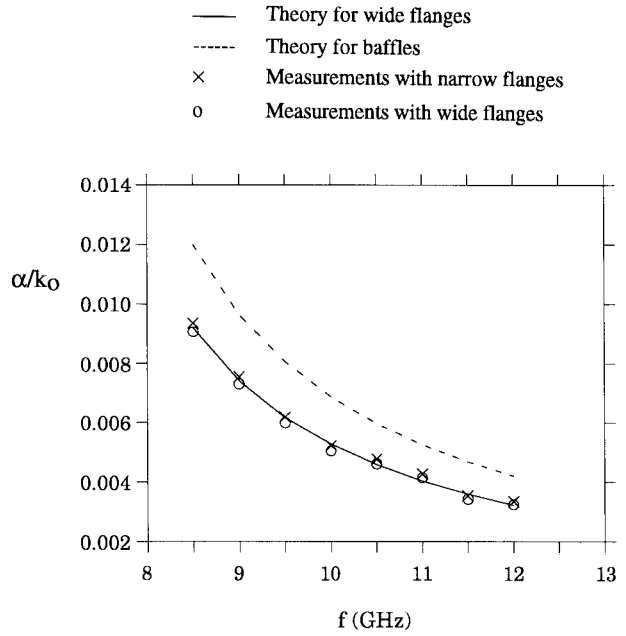

Fig. 10. Same as for Fig. 9, but for the normalized leakage constant. Results are shown for various terminations on the stub guide.

is a systematic difference between the values of α/k_o for narrow flanges and for very wide ones, with the narrow flanges yielding slightly higher values of α/k_o.

Two theoretical curves are presented in Fig. 10; the solid and dashed curves represent, respectively, the results when a ground plane (wide flanges) or a pair of baffles terminates the stub guide. It is interesting that the difference between those two curves is so pronounced, particularly when the corresponding difference was found to be negligible for β/k_o. Since the pair of baffles may be viewed as the extreme case of narrow flanges, it is important that the direction of the difference agrees with what was found for the measurements discussed just above.

It is also clear from Fig. 10 that the measured results again *agree very well* with the theoretical values. Since the leakage constant is seen to be much more sensitive than the phase constant, the very good agreement in Fig. 10 is an even better verification of the validity of the theory employed.

V. Radiation Patterns

As indicated in Section III-B, radiation pattern measurements were taken in both the millimeter wave and the X-band frequency ranges. For both frequency ranges, however, the distances between the transmitting and receiving antennas were too short to allow far-field measurements to be taken, so that measurements in the *near field* were all that could be obtained. For the millimeter-wave range, calculations were also made of the near-field patterns and comparisons are presented below of calculated and measured patterns.

Since the measured patterns in the two frequency ranges are qualitatively similar to each other and since calculations were made only for the millimeter wave range, the discussion below focuses on that range and only brief remarks are made

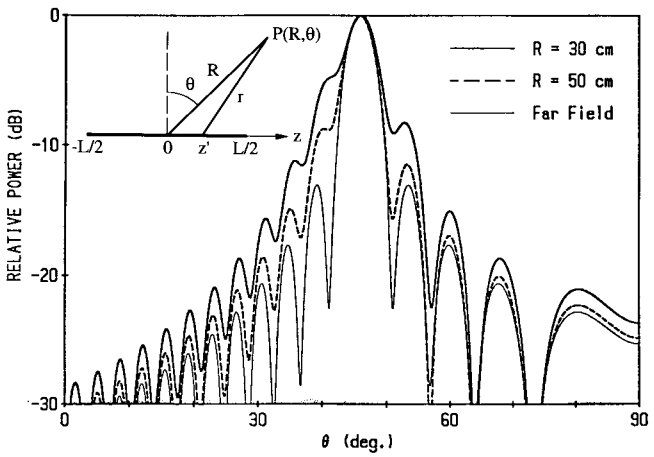

Fig. 11. Calculated near-field power patterns at the mid-range frequency 50 GHz for several distances R from the antenna. The distances here are 30 and 50 cm and the patterns for them are compared with the far-field pattern.

for the X-band range. Some X-band pattern measurements were included in [4] (in Italian), referred to earlier.

A. Calculations for the Near-Field Patterns

The measurements at millimeter wavelengths were all taken at a distance of 30 cm from the center of the antenna aperture. Using the far-field criterion, $R \cong 2L^2/\lambda_o$, where R is the distance in question, $L = 10$ cm is the antenna aperture length, and $\lambda_o = 6$ mm is the wavelength at the mid-range frequency 50 GHz, we find $R = 333$ cm so that the pick-up horn should be located at least that distance away to be at the beginning of the far field. We note that the minimum distance for far-field measurements would be about ten times the distance available to us for these measurements.

Before being able to compare measured with theoretical results, we must, therefore, compute the field patterns one should expect to find in the *near field* rather than those in the far field. For the measurements of the field patterns, a matched load was placed at the end of the antenna aperture. The aperture field distribution along the propagation direction z is of the form

$$e^{-j(\beta - j\alpha)z}. \tag{1}$$

The near-field pattern in the principal plane is then given approximately by

$$F(R,\theta) \cong \left| \int_{-\frac{L}{2}}^{\frac{L}{2}} e^{-j(\beta - j\alpha)z'} \frac{e^{-jk_o r}}{r}\, dz' \right|^2 \tag{2}$$

where

$$r^2 = R^2 + (z')^2 - 2Rz' \sin\theta \tag{3}$$

and the various symbols are defined in the sketch in the inset in Fig. 11. In the integration, we do not approximate (3) for r. From (2) and (3) we see that the pattern shape should be a function of distance R.

Calculated near-field power patterns at 50 GHz as a function of angle θ at distances R equal to 30 and 50 cm are presented in Fig. 11. (Curves for 70, 100, and 200 cm are presented in

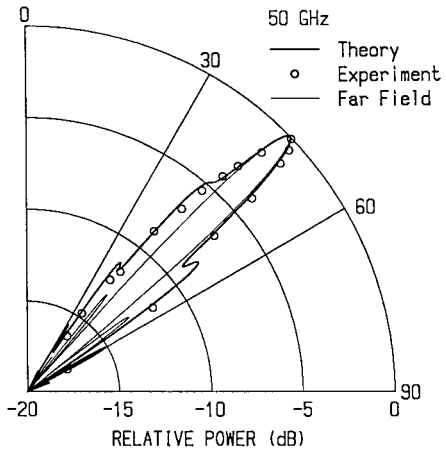

Fig. 12. Comparison at 50 GHz between the theoretical near-field pattern (solid curve) and measured values (hollow points) employing a polar-power plot. The distance from the antenna is 30 cm. A fine line curve representing the far-field pattern is added here.

[6].) On the plot there also appears a fine line curve, which represents the *far*-field pattern. It is seen that in the near field the sidelobes are higher, the dips fill differently, and the beam width increases a bit.

B. Comparisons Between Measurements and Theory

A polar plot of the near-field pattern at $R = 30$ cm is presented in Fig. 12 for a frequency equal to 50 GHz. (Plots for the additional frequencies 41, 45, 55, and 58 GHz may be found in [6].) The solid line on this plot represents the theoretical near-field calculation based on (2) and (3); the points correspond to measured results obtained by using the setup discussed in Section III-B. We have also included a fine line drawing that corresponds to the far-field calculation at that frequency.

Inspection of the plot in Fig. 12 reveals that the points agree very well with the theoretical curve. Although both the measured and the theoretical results hold for the near field at the distance $R = 30$ cm, their good agreement suggests that the far-field calculations employing the appropriate α and β values should also be accurate. Near-field plots are generally somewhat ugly, but it should be clear that the far-field patterns are smooth and clean, as is borne out by the fine-line far-field plot appearing in Fig. 12.

Measured near-field patterns were also obtained in the X-band frequency range, at the following frequencies: 8.5, 9.5, 10.0, 10.5, 11.5, and 12.4 GHz. Detailed plots in both rectangular and polar forms are presented in [4] for the frequencies 8.5, 10.0, and 12.4 GHz. Since no calculated patterns are available for comparison with these measurements and since these measured patterns are qualitatively similar to those appearing in Fig. 12, none of these patterns are shown here.

The angle θ_m of the maximum of each of these beams is the same as the angle we would find for the far-field patterns, as seen from Figs. 11 and 12. That angle can be obtained directly from polar plots similar to the one in Fig. 12 and it can be calculated from the value of β/k_o making use of the simple relation (1) of Part I, namely

$$\sin\theta_m \cong \frac{\beta}{k_o}. \tag{4}$$

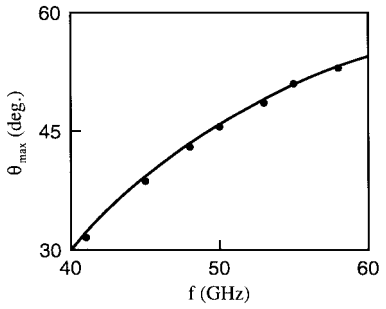

Fig. 13. Variation with frequency of the angle θ_m of the beam maximum. The solid line represents the approximate theoretical values obtained from (4) and the points correspond to the measured values.

In Fig. 13 we present a solid curve representing the theoretical values of θ_m obtained via (4) and a set of solid points that correspond to the peak in the measured pattern in Fig. 12 and from corresponding patterns at other frequencies. Although the agreement is seen to be rather good, the approximate values from (4) yield angles that are very slightly further from broadside. The extremely simple relation (4) is very good when the leakage constant is not large.

VI. Conclusion

The purpose of Part III was to take appropriate measurements in order to verify the validity of the theoretical expressions derived in Parts I [1] and II [2]. Measurements were made of the propagation wavenumbers β and α and of radiation patterns. These measurements were first made in the millimeter wave range from 40 to 60 GHz. Although *very good* agreement was obtained with the theoretical values in all cases, we found some scatter in the measured points for the values of β and α, which we attributed to the difficulty in making precise measurements at these small wavelengths. We, therefore, conducted a second set of measurements at X-band from roughly 8 to 12 GHz, where all dimensions are larger by about a factor of five. Less scatter was found in the measured data and the agreement with theory was again very good.

The two antenna structures that were built for measurements in these two frequency ranges are described in Section II, and the measurement methods employed are discussed in Section III. The comparisons with theory for the propagation wavenumbers β and α are presented in Section IV and those for the radiation patterns are given in Section V.

The principal conclusion to be drawn from these comparisons is that in *all* cases, the agreements between measurements and theory are *very good*, thereby verifying that the theoretical expressions in Parts I and II are accurate and reliable.

Additional interesting information was obtained from the measurements of β and α in the X-band frequency range. The stub-guide portion of the leaky-wave antenna may be terminated by a pair of baffles or by flanges, which can be narrow or wide approximating a ground plane. Expressions

were derived in Part II for the effects on β/k_o and α/k_o when the termination is a pair of baffles or is a ground plane. However, it would also be valuable to know how the β/k_o and α/k_o values are modified when the flanges are changed from narrow to wide.

As discussed in detail in Section IV-B, the measurements made in the X-band range do in fact provide such additional information. The results are that the values of β/k_o remain essentially the same, but the values of α/k_o do change slightly, yet noticeably, with the narrow flanges yielding slightly *higher* values of α/k_o. Calculations were also made to determine the differences produced when the flanges are replaced by a pair of baffles, which may be viewed as the extreme case of narrow flanges. It was found that the values of β/k_o were again affected negligibly, but those of α/k_o were influenced in a substantial way and in the same direction as that found experimentally when wide flanges were replaced by narrow ones. Since the values of the leakage constant *are* influenced by the geometry of the termination on the stub guide, one must take this aspect into account in the design.

ACKNOWLEDGMENT

The authors would like to thank R. Antonazzi and Alenia S.p.A. for their help in connection with the measurements in the X-band range.

REFERENCES

[1] P. Lampariello, F. Frezza, H. Shigesawa, M. Tsuji, and A. A. Oliner, "A versatile leaky-wave antenna based on stub-loaded rectangular waveguide: Part I—Theory," this issue, pp. 1032–1041.

[2] F. Frezza, P. Lampariello, H. Shigesawa, M. Tsuji, and A. A. Oliner, "A versatile leaky-wave antenna based on stub-loaded rectangular waveguide: Part II—Effects of flanges and finite stub length," this issue, pp. 1042–1046.

[3] G. A. Deschamps, "Determination of reflection coefficients and insertion loss of a waveguide junction," *J. Appl. Phys.*, vol. 24, pp. 1046–1050, Aug. 1953.

[4] R. Antonazzi, F. Frezza, P. Lampariello, R. Scarpetta, and A. A. Oliner, "Indagine sperimentale su antenne a onda leaky basate su guida rettangolare caricata da stub," in *Dig. IX Meet. Appl. Electromagn.*, Assisi, Italy, Oct. 1992, pp. 263–266.

[5] H. Shigesawa, M. Tsuji, P. Lampariello, F. Frezza, and A. A. Oliner, "Coupling between different leaky-mode types in stub-loaded leaky waveguides," *IEEE Trans. Microwave Theory Tech.*, vol. 42, pp. 1548–1560, Aug. 1994.

[6] A. A. Oliner, "Scannable millimeter wave arrays," Final Rep. RADC, Polytechnic University, Brooklyn, NY, Contract F19 628-84-K-0025, Sept. 1988, ch. VIII.

Mikio Tsuji (S'77–M'82), for a photograph and biography, see this issue, p. 1041.

Hiroshi Shigesawa (S'62–M'63–SM'85–F'94), for a photograph and biography, see this issue, p. 1040.

Fabrizio Frezza (S'87–M'92–SM'95), for a photograph and biography, see this issue, p. 1040.

Paolo Lampariello (M'73–SM'82–F'96), for a photograph and biography, see this issue, p. 1040.

Arthur A. Oliner (M'47–SM'52–F'61–LF'87), for a photograph and biography, see this issue, p. 1041.